www.czasopisma.pan.pl PAN POLSKA AKADEMIA NAUK www.journals.pan.pl

Arch. Min. Sci. **67** (2022), 4, 743-756

Electronic version (in color) of this paper is available: http://mining.archives.pl

DOI: https://doi.org/10.24425/ams.2022.143685

MARIUSZ MŁYNARCZUK[1], MARTA SKIBA[2*]

AN APPROACH TO DETECT LOCAL TECTONIC DISLOCATIONS IN COAL SEAMS BASED ON ROUGHNESS ANALYSIS

The occurrence of faults in coal seams has an impact on the possibility of methane hazard. There are several methods for identifying tectonic faults, but they cannot be applied directly to solve dynamic hazard problems in coal mine. Thus, searching for appropriate methods, that can detect faults in regional and local scales is needed. In order to meet this need, the paper proposes a new measurement method of estimating changes to the coal structure, based on profilometry measurements (roughness analysis) and application of madogram functions. Based on examining coal samples from near fault zones it was shown that the proposed approach allows us to detect changes of the coal surface that appear as the distance to a tectonic fault gets shorter. The proposed method, due to its simplicity and speed of measurement, implies a potential for practical application in the process of detecting local tectonic dislocations in coal mines.

Keywords: local tectonic fault; mining hazards; roughness; madogram; geostatistic; mathematical morphology

1. Introduction

The extraction of hard coal is inextricably connected with the occurrence of various natural threats, including threats related to the occurrence of gases [1]. One of them are gas and rock outbursts. Due to the significance of this threat and tragic consequences that it entails, an ongoing monitoring process aimed at determining the level of threat from this phenomenon is under way [2]. Still, such monitoring proves ineffective when we encounter the so-called gas traps

[1] AGH UNIVERSITY OF SCIENCE AND TECHNOLOGY, FACULTY OF GEOLOGY, GEOPHYSICS AND ENVIRONMENTAL PROTECTION, AL. MICKIEWICZA 30, 30-059 KRAKOW, POLAND

[2] STRATA MECHANICS RESEARCH INSTITUTE OF THE POLISH ACADEMY OF SCIENCES, REYMONTA 27, 30-059 KRAKOW, POLAND

* Corresponding author: skiba@imgpan.pl

(or gas pockets). They are characterized by increased gas capacity, tightened gas pressure and different structural properties of coal. Most frequently, they occur in the area of tectonic faults. In such spots, the so-called tectonically deformed coal, sheared coal or structurally altered coal, occurs [3-7]. In the paper by Skiba et al. [8] a method for the automatic classification of structurally deformed coal with the use of artificial neural networks was proposed. These geological structures not only change the coal seam stress and gas environment, but more importantly, they change the coal microstructure (matrix, pore, crack, etc.), and further change the coal characteristics [2,9-11]. According to Cao et al. [12] outbursts always occurred within a zone of tectonic coal surrounding the fault. As the scale of the current plate tectonics is large, it cannot be applied directly to solve the dynamic hazard problems in a coal mine. Hence, the methods that can identify and detect faults in regional and local scales are needed [13-15].

Over the years, many researchers have worked on fault identification and detection methods. Among them, the following should be mentioned: grid-based ensemble Kalman filter [16], curvature [17], seismic and scattered data analysis [18,19], integration of remote sensing and geographic information systems [20] or temperature vegetation dryness index [21].

It is worth paying attention to the work of Chen et al. [15], in which the authors proposed the mapping technology as a fault identification method. It is based on topographic and geomorphic analyses to identify the development of regional faults. In the paper authors also compared the obtained results with historical coal and gas outbursts and were indicated that more than 90% of the coal and gas outbursts occurred in the vicinity of faults, especially at the intersections of multiple faults and in areas with concentrated faults.

The possibilities of using stereological methods in the process of detecting local faults characterized by the presence of tectonically deformed coal were also discussed in the open literature [22]. However, these methods – based on the microscopic analysis – are of little use when it comes to the ongoing prevention activities in mines. This is due to the fact that they require preparing special coal microsections, as well as conducting a significant number of arduous and time-consuming quantitative measurements.

Therefore, finding measurement methods that would make it possible to faster detect local differences in the coal structure is still an essential task. Authors of this study concluded that an analysis of the roughness of coal samples can be such a method. While looking into the issue of surface shape of coal samples, one is tempted to think that the coal occurring in near-fault zones (structurally deformed coal) should display a surface shape that is a little different from the surface shape of an undeformed coal. In the presented work, appropriate research was conducted to verify that hypothesis.

2. Materials and methods

2.1. The origin of the research material

For the purpose of the research, the following coal material collected from three mines of the Upper Silesian Coal Basin, Poland. The selected faults were sampled from both sides (right and left) and from around the fault fracture. Lump samples were taken that were large enough to be placed under the laser profilometer (no smaller than 2×2×2 cm). Their orientation with respect to the fault was marked for later orientation under the profilometer. It needs to be stated

that the samples were collected under mine conditions, during the regular working hours of the facility. Therefore, the locations mentioned above should be treated as approximations. The samples were collected at small, local tectonic dislocations, whose thrust did not exceed 0.5 m. The samples were collected in:

1) Coal Mine A:
   A series of three minor local tectonic dislocations was encountered. In the near-fault zones, the following coal samples were collected (the mean reflectance of vitrinite, Ro = 0,79%, volatile matter content, V_{daf} ~26%):
   - in the area of the fault no. 1: from the spots located 10, 5, 2 and 1 meter to the left, from the fault fissure (marked as 0 m), and from the spots located 10, 5, 2 and 1 meter to the right,
   - in the area of the fault no. 2: from the spots located 10, 5, 2 and 1 meter to the right and from the fault fissure (marked as 0 m),
   - in the area of the fault no. 3: from the spots located 10, 5, 2 and 1 meter to the left, from the fault fissure (marked as 0), and from the spots located 10, 5, 2 and 1 meter to the right.
2) Coal Mine B (the mean reflectance of vitrinite, Ro = 0,98%, volatile matter content, V_{daf} ~30%):
   A tectonic discontinuity was observed from which samples were collected: from the spots located 10, 5, 3 and 1.5 meter to the left, from the fault fissure (marked as 0 m), and from the spots located 10, 5, 2 and 1 meter to the right.
3) Coal Mine C (the mean reflectance of vitrinite, Ro = 1,17%, volatile matter content, V_{daf} ~25%):
   Samples were collected from the spots located 10, 5, 2 and 1 meter to the left, as well as from the spots located 10, 5, 2 and 1 meter to the right of the tectonic fault.

2.2. Data acquisition

Over the past several years, the issue of rock fracture morphology has been discussed in works related to geology and rock mechanics more and more frequently. Application of laser profilometers to that end should be emphasized at this point. In the research described in this paper, a laser profilometry stand was used, composed of a laser head of the accuracy of 2 µm and measuring range of 5000 µm, a stepping table with the step of 1 µm and range of 50×50 mm, and a computer with controlling software.

Prior to the measurement, a coal sample had to be placed manually upon the measurement table. The researcher attempted to do it in such a way as to make the median plane of the sample's surface parallel to the plane of the table's shift. Any errors resulting from inaccurate leveling of samples were corrected based on the previously determined regression plane. The sample was placed upon a table in such a way as to make the measured axis X overlap the bedding direction observed on the coal sample. One feature of the used equipment is that it is sometimes unable to obtain information as to the measured point (e.g. when the surface inclines too much or when the light reflection index has too small a value). The unmeasurable points were approximated by means of the ordinary kriging method [23].

After the instrument completed the task, a table of XYZ coordinates of the measured points of the sample's surface was obtained. The data from the table may be processed and presented in

many ways, including presenting the data in the form of an image. Under such an approach, each piece of the measurement data can be recorded as one pixel of a picture, in such a manner that the location of that pixel's X and Y will correlate with the location of the measured point, and the grayness level of the pixel will correspond to the measured Z value. This approach makes it possible to analyze a rock fracture using the entire mathematical apparatus applied in the standard methods of image transformation and analysis, and in mathematical morphology.

2.3. Roughness and waviness

Upon launching an analysis of the shape of a surface, one should remember that the measured original surface should be viewed as a combination of two basic components: the waviness component and roughness component [24,25].

One of the essential problems connected with the interpretation of the roughness of rock fractures is defining the filter determining the borderline between roughness and waviness. The impact of the filtration size on the changes of basic parameters of linear roughness as defined by ISO was analyzed by Gurau et al. [26]. Selected scientific works suggest using various filtrations to this end, including Fourier transform [27] and wavelets [28], etc. Many authors rely on the filtration proposed in ISO standards [24,29]. Some other, non-standard methods of profile filtration are also being suggested. Chen et al. [30] propose their own 3D filtration model, and Młynarczuk [31] suggested the application of filters used in mathematical morphology.

A morphological filter is defined as an increasing and idempotent transformation. The simplest morphological filters include opening (1) and closing (2) [32]. They are the composition of erosion and dilation [33] and are defined as follows:

$$\gamma_B(f) = \delta_B(f)\,\varepsilon_{B^T}(f) \tag{1}$$

$$\varphi_B(f) = \varepsilon_B(f)\,\delta_{B^T}(f) \tag{2}$$

where: $\varepsilon(f)$, $\delta(f)$ – erosion and dilatation of function f, B – structuring element, B^T – symmetric structuring element.

Combining two morphological filters characterized by an increasing size of the structural element B_n lets us obtain the so-called alternating sequential filters-ASF [34]. In the discussed research, the authors used one of the varieties of this filter, defined as:

$$M_i(f) = \varphi_{Bi}(f)\,\gamma_{Bi}(f)\ldots\varphi_{B2}(f)\,\gamma_{B2}(f)\,\varphi_{B1}(f)\,\gamma_{B1}(f) \tag{3}$$

2.4. Variogram and madogram

In the analysis of the surface shape or texture, the variogram function is frequently used [35-37]. Variogram is defined as:

$$2\gamma(h,\alpha) = \frac{1}{N}\sum_{i=1}^{N}\left(Z(x_i) - Z(x_i + h)\right)^2 \tag{4}$$

where: h is the lag distance – in direction α – between two points, $Z(x_i)$ and $Z(x_i + h)$.

There are three parameters characteristic for the semivariogram i.e. the nugget, the sill and the range (Fig. 1). When the semivariogram starting from a non-zero value, this value is called the nugget effect. It expresses the variability of quantity at a scale smaller than the sampling interval. It can also be caused by low measurement accuracy. The value reached by the semivariogram at which no further increase of the function is observed is called sill. It is approximately equal to the sampling variance. The distance from zero to the point where semivariogram reaching the 95% of the sill is called the range. It states the largest distance at which the sampled values are correlated with each other [38].

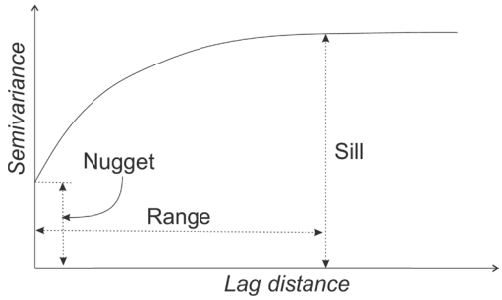

Fig. 1. Important characteristics of a semivariogram (own elaboration)

In the discussed research, a variogram version known as madogram was used. The madogram is first-order variogram, defined similarly to the variogram, with the only difference being the fact that the square of the difference between the grayness levels of a pair of pixels is replaced with a module (Eq. 5).

$$2\gamma_1(h,\alpha) = \frac{1}{N}\sum_{i=1}^{N}\left|Z(x_i) - Z(x_i + h)\right| \tag{5}$$

In the presented research, particular attention was paid to the madogram's sill, i.e. the value at which a function does not display further growth, having reached that value [39]. Madograms are less sensitive to extreme values than variograms. They can be useful in the process of concluding about the anisotropy of data sets revealing outliers which are hard to interpret by means of variograms [29].

2.5. Measurement procedure

Finally, the measurement procedure was as below (Fig. 2):

- From the material collected in the vicinity of the analyzed faults, samples were selected, and the shape of these samples was mapped using a laser profilometer (the samples were placed to make the measured axis X overlap the bedding direction).
- Fields of 256×256 points, located 20 μm apart from each other, were measured. This resulted in the total of 65,536 measurement points placed on a field of 5.1×5.1 mm in size.
- Unmeasurable points were approximated using the kriging method.

- Errors caused by inappropriate positioning of the median plane of the samples surface in relation to the plane of the table shift were eliminated by determining the regression level and making appropriate corrections.
- The measurement data was converted into a bit map (a gray image).
- The initial filtration of measurement data was performed in order to eliminate the measurement noise.
- To identify the roughness components of the measured surfaces, the obtained data was filtered using alternating sequential filters of the size of 20 pixels (400 μm). The filter result was subtracted from the obtained data.
- Madograms heading towards the X axis were determined on the obtained images.

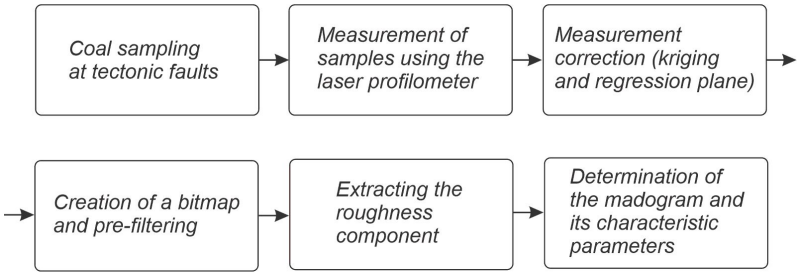

Fig. 2. Schematic diagram of the measurement procedure

3. Measurement results

Figs 3-5 present madograms for the coal samples collected in the Coal Mine A, where a series of three local tectonic dislocations was encountered. It needs to be stated that the distance between the 2nd and 3rd fault was ca. 14 m, which is why the samples collected in the spot located 10 m away to the left side of the fault no. 3 corresponded to the samples collected in the spot located some 5 m away to the right side of the fault no. 2. This could have led to certain misreadings of the results obtained for the left side of fault no. 3 and the right side of fault no. 2.

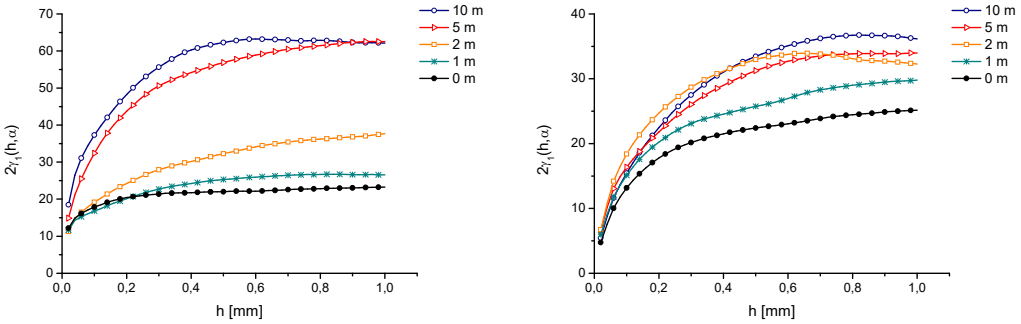

Fig. 3. Madograms for the Coal Mine A, fault no. 1: a) left side (hanging wing), b) right side (footwall wing)

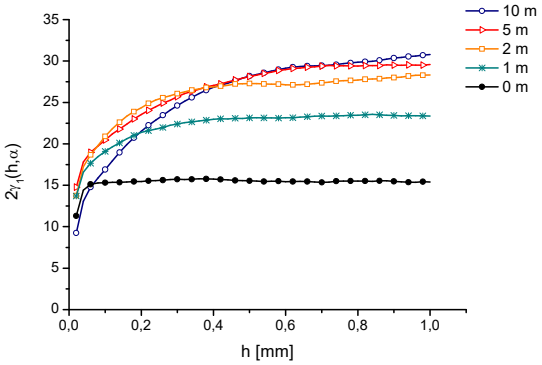

Fig. 4. Madogram for the Coal Mine A, fault no. 2 – right side (hanging wing)

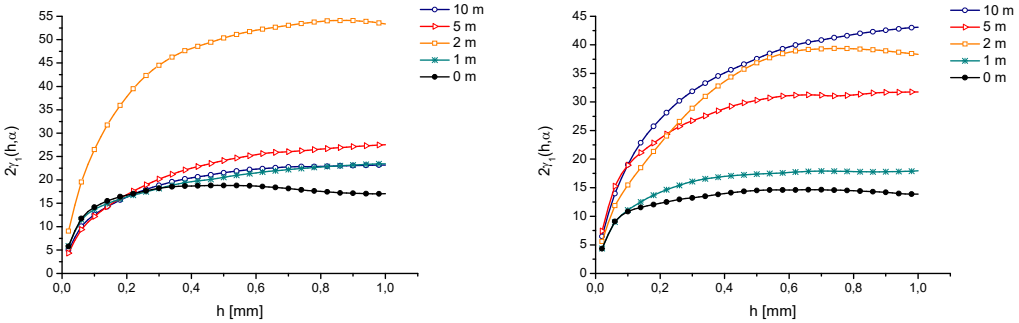

Fig. 5. Madograms for the Coal Mine A, fault no. 3: a) left side (footwall wing), b) right side (hanging wing)

It can be observed that, in the case of the samples collected in the vicinity of fault no. 1 and fault no. 2, the madogram sills are largely dependent on the spot where they were collected. The madogram sills obtained for the samples collected to the right side of fault no. 3 also decrease as the distance to the fault is reduced, with the only exception being a sample collected in a spot located 2 m away from the fault. Some poorer results were obtained for the left side of fault no. 3, where the sample collected in the spot located 2 m away from the fault displays parameters that differ significantly from the expected ones, and madogram sills for other samples are not distinctly separated.

When analyzing how the madogram course changes with the distance to the fault, one should pay attention to the fact that, in the majority of cases, such a relationship does occur. Still, such an analysis should be limited only to studying the local changeability within a single fault, or even in relation to one side of a fault. At the same time, madogram courses for various faults should not be compared.

The values of madograms determined for the samples collected in the Coal Mine B are presented in Fig. 6.

The results are the worst that have been obtained during the discussed analysis, as the madogram sill is not fully related to the distance from the spot where a sample was collected. Still, it was

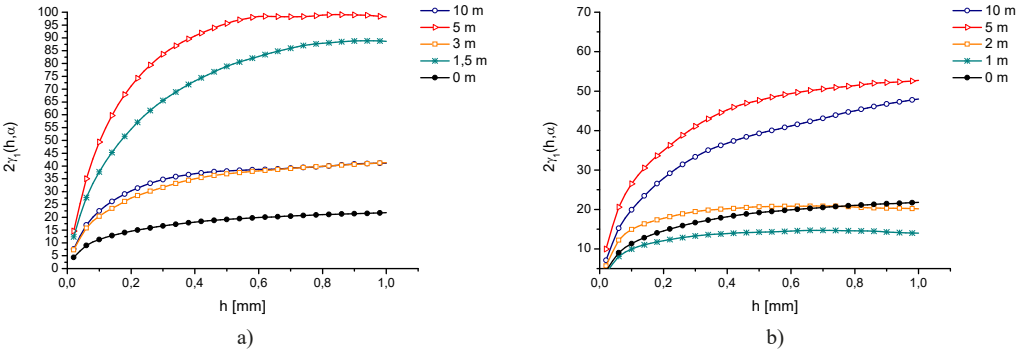

Fig. 6. Madograms for the Coal Mine B: a) left side (footwall wing), b) right side (hanging wing)

confirmed that the madogram sills of the samples collected in spots located significantly further from a fault (i.e. ca. 5-10 m) are higher than those of the samples collected in the direct vicinity of a fault. This relationship is manifested in virtually all samples analyzed in the present paper.

In the Coal Mine C, eight coal samples were collected: four from the area to the left side of a fault, and four from the area to the right side of a fault. An attempt to collect a solid sample from the fault itself (at a 0 m) ended in a failure. Fig. 7 presents madogram values determined for these samples.

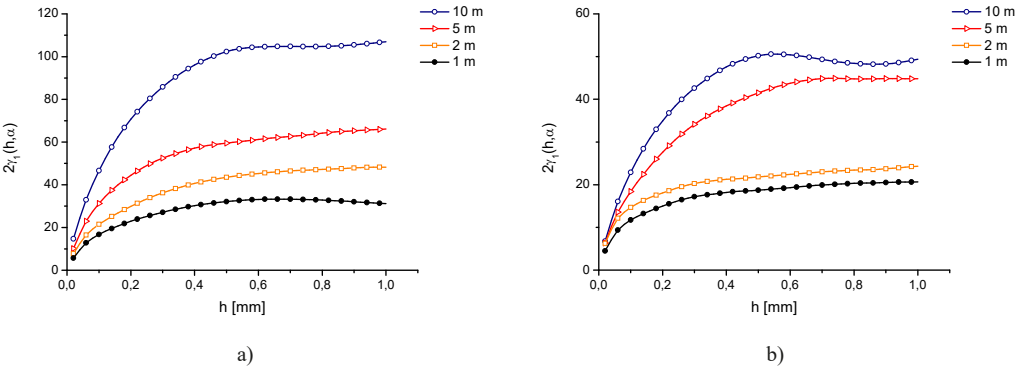

Fig. 7. Madograms for the Coal Mine C: a) left side (footwall wing), b) right side (hanging wing)

When analyzing the results obtained for the samples collected in the Coal Mine C, it can clearly be seen that madogram sills determined for these samples decrease as the distance between the spot at which they were collected, and the fault gets reduced.

The obtained results point to a relationship between the madogram sill and the distance of the collected sample from a fault. For the majority of the samples collected in the Coal Mine A, for both series of the samples collected in the Coal Mine C and (to a slightly lesser extent) for one series of the samples collected in the Coal Mine B, one can observe a visible trend involving decreasing the madogram sill with the diminishing distance to the fault. Therefore, it seems that there exists a measurable relationship between the shape of a coal fracture surface and a distance

from the fault, and the discussed measurement method makes it possible to describe these changes in a quantitative way, in the majority of cases.

The next stage of the research was to fit the model curves to the measurement data. The results of this model fit are presented in Figs 8-12.

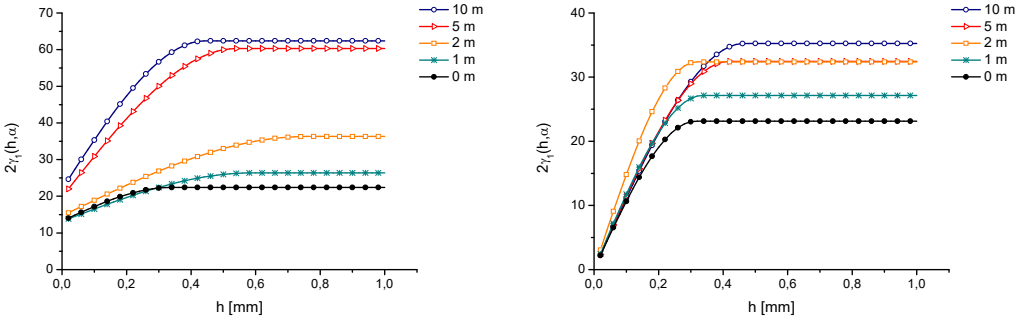

a) b)

Fig. 8. Results of the model curves fit for the Coal Mine A, fault no. 1: a) left side (hanging wing), b) right side (footwall wing)

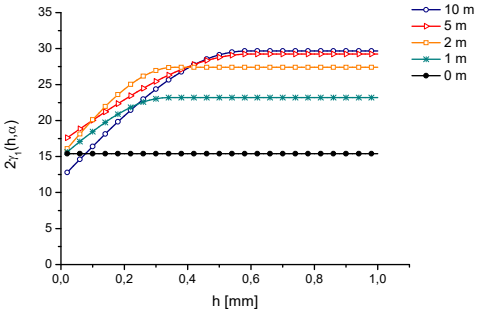

Fig. 9. Results of the model curves fit for the Coal Mine A, fault no. 2 – right side (hanging wing)

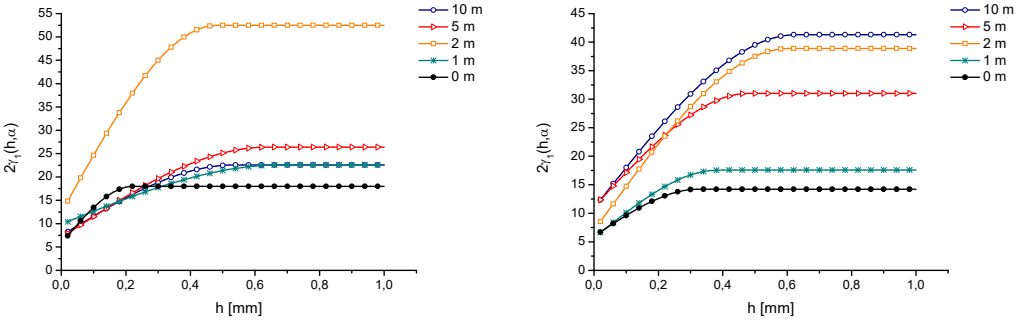

a) b)

Fig. 10. Results of the model curves fit for the Coal Mine A, fault no. 3: a) left side (footwall wing), b) right side (hanging wing)

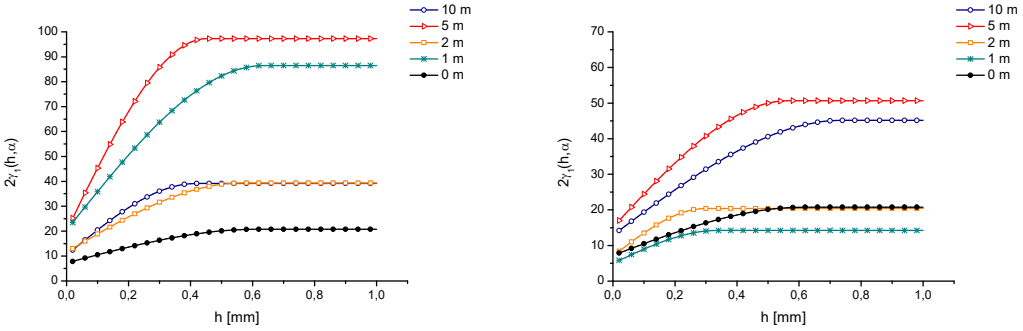

Fig. 11. Results of the model curves fit for the Coal Mine B: a) left side (footwall wing), b) right side (hanging wing)

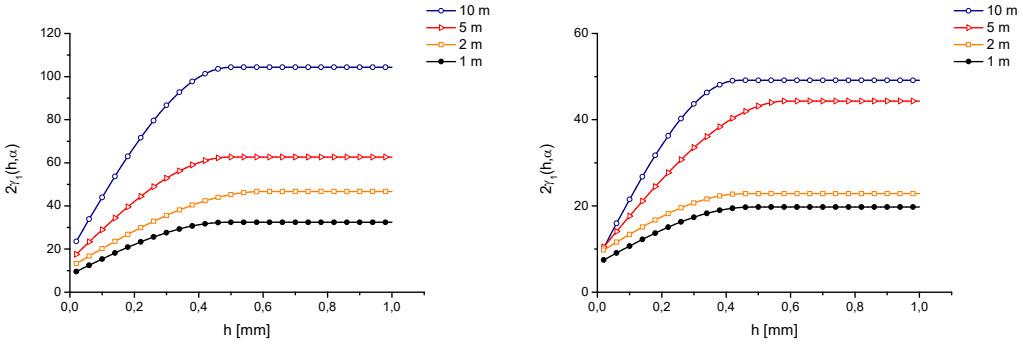

Fig. 12. Results of the model curves fit for the Coal Mine C: a) left side (footwall wing), b) right side (hanging wing)

As a result of fitting the model curves to the measurement data, information on the values of the madogram thresholds was obtained. The results are presented in Tables 1-3.

The analysis of the obtained results also shows that, for all the discussed cases, the madogram sills of the samples collected in the spots located furthest from the fault (i.e. 10 m away) are higher than madogram sills of the samples collected in a fault itself. This relationship is presented in

TABLE 1

Madogram sills for samples from the Coal Mine A

	10 m	**5 m**	**2 m**	**1 m**	**0 m**
fault 1 – left [µm]	62.4	60.3	36.3	26.4	22.4
fault 1 – right [µm]	36.0	33.4	33.0	28.5	23.8
fault 2 – right [µm]	29.7	29.3	27.4	23.2	15.4
fault 3 – left [µm]	22.6	26.4	52.5	22.6	18.0
fault 3 – right [µm]	41.3	31.0	38.9	17.6	14.2

TABLE 2

Madogram sills for samples from the Coal Mine B

	10 m	5 m	2 m	1 m	0 m
fault – left [µm]	39.1	97.3	39.3	86.5	20.7
fault – right [µm]	45.2	50.7	20.4	14.2	20.7

TABLE 3

Madogram sills for samples from the Coal Mine C

	10 m	5 m	2 m	1 m
fault - left [µm]	104.3	62.7	46.7	32.4
fault - right [µm]	49.1	44.3	22.8	19.7

Table 4. At this point, it needs to be stated that the measurement data in this research was matched with model curves based on which the madogram sills were established. When analyzing the faults, one can see that in the immediate vicinity of the faults (0 m-1 m), the madograms have higher values in the footwalls (see Table 1). This observation should be the subject of further research.

TABLE 4

The relationship between the madogram sill established for the samples collected in the spots located 10 m away from the fissure and madogram sill established for the samples collected in the direct vicinity of the fissure (0 m for the Coal Mines A and B, and 1 m for the Coal Mine C)

	Coal Mine A					Coal Mine B		Coal Mine C	
Place of measuring	fault no. 1 – left	fault no. 1 – right	fault no. 2 – right	fault no. 3 – left	fault no. 3 – right	fault – left	fault – right	fault – left	fault – right
Madogram sill (10 m)/ madogram sill (fissure)	2.8	1.5	1.9	1.3	2.9	1.9	2.2	3.2	2.5

4. Conclusions

In the described research, a new measurement procedure was proposed, which allows to indicate the approaching local tectonic fault, based on the analysis of the coal surface. As part of the research, appropriate profilometric measurements were carried out, roughness components were extracted and then the madograms and its characteristic parameters were determined.

The analysis of the results shows that the distances from the fault at which a given coal samples were collected and the obtained values of madogram sills are interrelated. In all the analyzed cases, the madogram sills for the coal samples collected at the fault are below the madogram sills obtained for coals located away from the faults. It was also observed that, in a lot of cases, the madogram sills decrease as the distance between the spot where a sample was collected, and a fault becomes shorter. For the tested coal samples, in the immediate vicinity of the fault, it was even a 3.2-fold decrease compared to the madogram sills determined at a distance of 10 m from the fault. Therefore, the authors believe, that the proposed measurement method can detect a change in the coal structure as the distance to the fault gets reduced.

The usefulness of the proposed method is also demonstrated by the fact that the measurements do not require lengthy preparations and may be conducted directly in the coal mine, even without collecting samples (i.e. directly on the side wall of longwalls or headings).

To summarize, it can be stated that the described measurements come as useful in the process of detecting local fault zones and may likely be applied to the task of evaluating the level of threat of rock and gas outbursts in coal mines.

Acknowledgements

The work was financed within the framework of the statutory research of the Strata Mechanics Research Institute of the Polish Academy of Sciences and the AGH-University of Science and Technology, Faculty of Geology, Geophysics and Environmental Protection. The research was also financed as part of a research project NR09-0038-06.

References

[1] W. Song, J. Cheng, W. Wang, Y. Qin, Z. Wang, M. Borowski, Y. Wang, P. Tukkaraja, Underground Mine gas explosion accidents and prevention techniques – an overview. Arch. Min. Sci. **66** (2), 297-312 (2021). DOI: https://doi.org/10.24425/ams.2021.137463

[2] D.J. Black, Review of coal and gas outburst in Australian underground coal mines. Int. J. Min. Sci. Technol. **29** (6), 815-824 (2019). DOI: https://doi.org/10.1016/j.ijmst.2019.01.007

[3] H. Li, Y. Ogawa, S. Shimada, Mechanism of methane flow through sheared coals and its role on methane recovery. Fuel **82**, 1271-1279 (2003). DOI: http://doi.org/10.1016/S0016-2361(03)00020-6

[4] N. Skoczylas, A. Pajdak, K. Kozieł, L. Braga, Methane emission during gas and rock outburst on the basis of the unipore model. Energies **12** (10), 1999 (2019). DOI: https://doi.org/10.3390/en12101999

[5] Q. Tu, Y. Cheng, T. Ren, Z. Wang, J. Lin, Y. Lei, Role of tectonic coal in coal and gas outburst behavior during coal mining. Rock Mech. Rock Eng. **52** (11), 4619-35 (2019). DOI: http://doi.org/10.1007/s00603-019-01846-0

[6] X. Pan, H. Cheng, J. Chen, X. Zhou, An experimental study of the mechanism of coal and gas outbursts in the tectonic regions. Eng. Geol. **279**, 105883 (2020). DOI: http://doi.org/10.1016/j.enggeo.2020.105883

[7] L. Wang, Z. Long, Y. Song, Z. Qu, Supercritical CO2 adsorption and desorption characteristics and pore structure controlling mechanism of tectonically deformed coals. Fuel **317**, 123485 (2022). DOI: http://doi.org/10.1016/j.fuel.2022.123485

[8] M. Skiba, K. Godyń, M. Młynarczuk, Identification of Structurally Altered Coal from Near-Fault Zones as Performed with Neural Classifiers. J. Min. Sci. **57** (5), 873-882 (2021). DOI: http://doi.org/10.1134/S1062739121050173

[9] F.H. An, Y.P. Cheng, An explanation of large-scale coal and gas outbursts in underground coal mines: the effect of low-permeability zones on abnormally abundant gas. Nat. Hazards Earth Syst. Sci. **1**, 4751-75 (2013). DOI: http://doi.org/10.5194/nhess-14-2125-2014

[10] W. Li, T. Ren, A. Busch, S.A.M. den Hartog, Y. Cheng, W. Qiao, B. Li, Architecture, stress state and permeability of a fault zone in Jiulishan coal mine, China: Implication for coal and gas outbursts. Int. J. Coal Geol. **198**, 1-13 (2018). DOI: http://doi.org/10.1016/j.coal.2018.09.002

[11] N. Skoczylas, A. Pajdak, M. Kudasik, L. Braga, CH4 and CO2 sorption and diffusion carried out in various temperatures on hard coal samples of various degrees of coalification. J. Nat. Gas Sci. Eng. **81**, 103449 (2020). DOI: http://doi.org/10.1016/j.jngse.2020.103449

[12] Y.X. Cao, D. He, G.C. David, Coal and gas outbursts in footwalls of reverse faults. Int. J. Coal Geol. **48**, 47-63 (2001). DOI: http://doi.org/10.1016/S0166-5162(01)00037-4

[13] Y. Cao, A. Davis, R. Liu, X. Liu, Y. Zhang, The influence of tectonic deformation on some geochemical properties of coals – a possible indicator of outburst potential. Int. J. Coal Geol. **53**, 69-79 (2003). DOI: http://doi.org/10.1016/S0166-5162(02)00077-0

[14] M. Młynarczuk, M. Wierzbicki, Stereological and profilometry methods in detection of structural deformations in coal samples collected from the rock and outburst zone in the "Zofiówka" Colliery. Arch. Min. Sci. **54** (2), 189-201 (2009).

[15] Y. Chen, F. Xie, X. Zhang, C. Wang, X. Xu, X. Wang, Y. Wang, Fault identification approach and its application for predicting coal. Arabian J. Geosci. **14**, 710 (2021). DOI: https://doi.org/10.1007/s12517-021-07042-1

[16] A.Y. Sun, Identification of geologic fault network geometry by using a grid-based ensemble kalman filter. J. Hazard. Toxic Radioact. Waste **15** (4), 228-233 (2011). DOI: http://doi.org/10.1061/(ASCE)HZ.1944-8376.0000072

[17] Z.H. Zheng, J.Q. Tan, K. Liu, Most extreme curvature and its application to seismic structural interpretation. Appl. Mech. Mater. **522-524**, 1266-1269 (2014).

DOI: http://doi.org/10.4028/www.scientific.net/AMM.522-524.1266

[18] H.Q Xu, S.Z. Sun, Z. Gui, S. Luo, Detection of sub-seismic fault footprint from signal-to-noise ratio based on wavelet modulus maximum in the tight reservoir. J. Appl. Geophys. **114**, 259-262 (2015).
DOI: http://doi.org/10.1016/j.jappgeo.2015.01.021

[19] M. Noori, H. Hassani, A. Javaherian, H. Amindavar, S. Torabi, Automatic fault detection in seismic data using Gaussian process regression. J. Appl. Geophys. **163**, 117-131 (2019).
DOI: http://doi.org/10.1016/j.jappgeo.2019.02.018

[20] M. Elhag, D. Alshamsi, Integration of remote sensing and geographic information systems for geological fault detection on the island of Crete, Greece. Geosciientific Instrumentation, Methods and Data Systems **8** (1), 45-54 (2019). DOI: http://doi.org/10.5194/gi-8-45-2019

[21] Ch. Wang, J. Chen, X. Chen, J. Chen, Identification of concealed faults in a grassland area in Inner Mongolia, China, using the temperature vegetation dryness index. J. Earth. Sci. **30** (4), 853-860 (2019).
DOI: http://doi.org/10.1007/s12583-017-0980-9

[22] R.D. Lama, J. Bodziony, Outburst of Gas, coal and Rock in Underground Coal Mines. R.D. Lama & Associates, Wollongong, NSW Australia (1996).

[23] H. Wackernagel, Multivariate geostatistics: an introduction with applications. Springer-Verlag Berlin Heidelberg GmbH (2003).

[24] A. Boryczko, Effect of waviness and roughness components on transverse profiles of turned surfaces. Measurement **46**, 688-696 (2013). DOI: http://doi.org/10.1016/j.measurement.2012.09.007

[25] S. Pomberger, M. Stoschka, M. Leitner, Cast surface texture characterisation via areal roughness. Precis. Eng. **60**, 465-481 (2019). DOI: http://doi.org/10.1016/j.precisioneng.2019.09.007

[26] L. Gurau, H. Mansfield-Williams, M. Irle, Filtering the roughness of a sanded wood surface. Holz als Roh- und Werkstoff **64**, 363-371 (2006). DOI: http://doi.org/10.1007/s00107-005-0089-1

[27] H. Hocheng, M.L. Hsieh, Signal analysis of surface roughness in diamond turning of lens molds. Int. J. Mach. Tools Manuf. **44**, 1607-1618 (2004). DOI: http://doi.org/10.1016/j.ijmachtools.2004.06.003

[28] Q. Chen, S. Yang, Z. Li, Surface roughness evaluation by using wavelets analysis, Precis. Eng. **23**, 209-212 (1999). DOI: http://doi.org/10.1016/S0141-6359(99)00013-6

[29] M. Młynarczuk, M. Skiba, L. Sitek, P. Hlaváček, A. Kožušníková, The research into the quality of rock surfaces obtained by abrasive water jet cutting. Arch. Min. Sci. **59** (4), 925-940 (2014).
DOI: http://doi.org/10.2478/amsc-2014-0064

[30] C.C.A Chen, W.C. Liu, N.A. Duffie, A Surface Topography Model for Automated Surface Finishing. Int. J. Mach. Tools Manufact. **38**, 543-550 (1998). DOI: http://doi.org/10.1016/S0890-6955(97)00100-4

[31] M. Młynarczuk, Description and classification of rock surfaces by means of laser profilometry and mathematical morphology. Int. J. Rock Mech. Min. Sci. **47** (1), 138-149. (2010). DOI: http://doi.org/10.1016/j.ijrmms.2009.09.004

[32] J. Serra, L. Vincent, An Overview of Morphological Filtering. Circuits Syst. Signal Process. **11** (1), 47-108 (1992). DOI: http://doi.org/10.1007/BF01189221

[33] J. Serra, Image Analysis and Mathematical Morphology, Academic Press, London (1982).

[34] J. Serra, Alternating sequential Filters, Image Analysis and Mathematical Morphology, Volume II, Theoretical Advances, ed. J. Serra, Academic Press, London (1988).

[35] U.C Herzfeld, C. Overbeck, Analysis and simulation of scale-dependent fractal surface with application to seafloor morphology. Comput. Geosci. **25**, 979-1007 (1999). DOI: http://doi.org/10.1016/S0098-3004(99)00062-X

[36] A. Marache, J. Riss, S. Gentier, J.P. Chiles, Characterization and reconstruction of a rock fracture surface by geostatistics. Int. J. Numer. Anal. Meth. Geomech. **26**, 873-896 (2002). DOI: http://doi.org/10.1002/nag.228

[37] S. Trevisani, M. Rocca, MAD: robust image texture analysis for applications in high resolution geomorphometry. Comput. Geosci. **81**, 78-92 (2015). DOI: http://doi.org/10.1016/j.cageo.2015.04.003

[38] J. Lipiec, B. Usowicz, Spatial relationships among cereal yields and selected soil physical and chemical properties. Sci. Total Environ. **633**, 1579-1590 (2018). DOI: https://doi.org/10.1016/j.scitotenv.2018.03.277

[39] S.J. Ha, Y.J. Jeong, T.S. Yun, Parameterization of the representative sizes of microstructural features in rocks using 3D X-ray computed tomographic images. Comput. Geosci. **144**, 104590 (2020). DOI: http://doi.org/10.1016/j.cageo.2020.104590